AASERT

FINAL TECHNICAL REPORT

Contract F49620-93-0353
(1 September 1993-31 August 1997)

AASERT Program

Principal Investigator: Jeffrey Bokor

Electronics Research Laboratory

University Of California, Berkeley

September 1997

REPORT DOCUMENTATION PAGE

Form Approved
OMB No. 0704-0188

1. AGENCY USE ONLY *(Leave Blank)*

2. REPORT DATE
30 September 1997

3. REPORT TYPE AND DATES COVERED
Final Technical 1 September 1993 - 31 August 1997

4. TITLE AND SUBTITLE
Femtosecond Laser Probing Of Non-Thermal Electronic Transport

5. FUNDING NUMBERS
61103D
3484/TS

6. AUTHORS
J. Bokor

7. PERFORMING ORGANIZATION NAME(S) AND ADDRESS(ES)
Electronics Research Laboratory
258 Cory Hall
University of California at Berkeley
Berkeley, CA 94720

8. PERFORMING ORGANIZATION REPORT NUMBER
UCB/ERL-97/1

9. SPONSORING / MONITORING AGENCY NAME(S) AND ADDRESS(ES)
AFOSR/NI
ATTN.: AASERT Program
110 Duncan Ave, Room B115
Bolling, AFB DC 20332-8050

10. SPONSORING / MONITORING AGENCY REPORT NUMBER
F49620-93-1-0353

11. SUPPLEMENTARY NOTES

12a. DISTRIBUTION / AVAILABILITY STATEMENT
APPROVED FOR PUBLIC RELEASE.
DISTRIBUTION UNLIMITED.

12b. DISTRIBUTION CODE

13. ABSTRACT *(Maximum 200 words)*
The goal of this research effort has been the application of high intensity THz pulses, generated by a large aperture planar photoconducting transmitter, in studying nonlinear phenomena in GaAs and Si. The ultimate interest in this is a better understanding of the response of free carriers in semiconductors to high electric fields, a subject of great importance in modern electronic devices. The THz generator offers the capability of producing a peak electric field in the range of 100 kV/cm, well into the range of high-field, hot carrier phenomena. In addition, due to the short duration of this pulse, the dynamics of carriers in high fields may be studied directly in the time domain, using the powerful techniques developed for femtosecond laser spectroscopy experiments. At high fields, carrier velocities become nonlinear in applied field. This forms the basis for the expectation of a nonlinear response of a doped semiconductor to a high intensity THz pulse passing through

14. SUBJECT TERMS
None

15. NUMBER OF PAGES

16. PRICE CODE

17. SECURITY CLASSIFICATION OF REPORT	18. SECURITY CLASSIFICATION OF THIS PAGE	19. SECURITY CLASSIFICATION OF ABSTRACT	20. LIMITATION OF ABSTRACT
UNCLASSIFIED	UNCLASSIFIED	UNCLASSIFIED	

NSN 7540-01-280-5500

Standard Form 298 (Rev. 2-89)
Prescribed by ANSI Std. Z39-1
298-102

FEMTOSECOND LASER PROBING OF NON-THERMAL ELECTRONIC TRANSPORT

AFOSR AASERT Grant: F49620-94-1-0353

Final Technical Report, Sept. 30, 1997

Principal Investigator: Jeffrey Bokor, EECS Department, University of California, Berkeley, CA 94720

Objectives

The goal of this research effort has been the application of high intensity THz pulses, generated by a large aperture planar photoconducting transmitter, in studying nonlinear phenomena in GaAs and Si. The ultimate interest in this is a better understanding of the response of free carriers in semiconductors to high electric fields, a subject of great importance in modern electronic devices. The THz generator offers the capability of producing a peak electric field in the range of 100 kV/cm, well into the range of high-field, hot carrier phenomena. In addition, due to the short duration of this pulse, the dynamics of carriers in high fields may be studied directly in the time domain, using the powerful techniques developed for femtosecond laser spectroscopy experiments. At high fields, carrier velocities become nonlinear in applied field. This forms the basis for the expectation of a nonlinear response of a doped semiconductor to a high intensity THz pulse passing through it.

Accomplishments/New Findings

Much effort has been necessary on the development of the transmitter itself, as well as improved detection and signal processing methods. During the first two years of this project, a careful study of the output and repetition-rate scaling characteristics of single 3 cm gap THz transmitters was completed, as well as a preliminary study of the propagation properties of the beam generated by these large aperture antennas. This work was reported in the M.S. thesis of Jeffrey Margolies, which is included with this report.

We showed, for the first time, that such large planar THz transmitters could be operated successfully at repetition rates above 10 Hz, up to 1 kHz. We also found that the saturation of the THz output with input visible laser pulse fluence depends on the pulse repetition rate. Previous studies of such transmitters had shown that the THz output energy increases with input visible laser fluence, but for fluence above about 40 microJoules/cm^2, the output saturates. We found that for high bias field (8-10 kV/cm), this saturation behavior is strongly modified when the pulse repetition rate is 1 kHz. Surprisingly, there is less saturation, and the energy per pulse is up to 60% higher at 1 kHz, compared to 10 Hz or 100 Hz repetition rate.

We also performed a study of the propagation properties of the THz beam. Beam profiles freely propagating from the antenna were measured, and they clearly reflect the presence of electric field enhancements near the bias electrodes. We attributed this enhancement to geometric enhancement of the bias field near the electrodes, and independently confirmed this by an electro-optic measurement of the bias field distribution. Profiles of the THz beam focused by a 2.5" focal length parabolic mirror were also measured revealing a focal spot size as small as 800 microns in diameter. The measured profile agreed quite accurately with a calculation based on broadband Fresnel diffraction theory. Propagation and focusing properties of the beam are important to understand quantitatively for accurate calculation of the electric field strength in the focus.

In the past year, we have continued to perfect the high power THz system for better data acquisition. An improvement has been achieved with the introduction of a new detection system based on the electro-optic effect, which permits a full detection of the amplitude and phase of the THz pulse. This new detector has enabled us to more completely characterize the propagation behavior of the THz pulses from the high-power large aperture antenna. In doing so, we also refined the simulation model for the THz beam propagation. Excellent agreement between measured and simulated THz pulse shapes were obtained, at various locations after the antenna, under different propagation conditions. The success of the simulation benefited from earlier results on the mapping of the applied bias field distribution inside the antenna gap. Two important new findings improve our understanding of the nature of THz pulse generation and propagation from the large gap antenna. The observed spatio-temporal profile of the THz pulse can only be understood in terms of the near-field propagation of an electrical pulse which is a replica of its generating current density at a distance very close to the antenna.

The focus of the effort has now shifted to the application of high intensity THz pulses, in studying nonlinear phenomena in GaAs, Si, and high-Tc superconductors $Bi_2Sr_2Ca_2Cu_3O_x$ (BSCCO) and $YBa_2Cu_3O_x$ (YBCO). The electro-optic detector is more broadband than our old Michelson interferometer, and as such, it allows a more sensitive detection of the nonlinear absorption, which occurs primarily at high frequencies. Experimental results of THz absorption by photogenerated carriers in semi-insulating GaAs have shown a decrease in absorption at frequencies above 1 THz as the THz pulse intensity is increased. It is consistent with our prediction based on a simulation model which was developed under the parent JSEP contract.

THz pulses are suitable probes for studying the dynamics of the superconducting electrons since their photon energies are less than the superconducting energy gap. Moreover, high intensity THz pulses allow us to probe the superconducting gap itself since there is enough energy in these pulses to break large numbers of Cooper pairs. The transmission of THz pulses through a superconductor is determined by the conductivity of the material, which in turn depends on the number of Cooper pairs. At temperatures below T_c, the transmission is low since there is a high density of Cooper pairs. As the THz pulses break these Cooper pairs, the transmission goes up. Hence, we expect to see a nonlinear transmission through the superconductor as a function of THz intensity for temperatures below T_c. Above T_c, the response is linear since there are no Cooper pairs.

In high-T_c superconductors such as BSCCO and YBCO, the energy gap is actually anisotropic in the momentum (**k**) space, i.e., the gap size is different along different

directions in the material. It has a four-fold symmetry with a vanishing energy gap at four points called nodes. The main motivation of this work is to map the gap anisotropy, which is difficult to probe using conventional electrical measurement techniques. Since the nonlinear response to the THz pulses is highly affected by the gap size, we can probe the gap anisotropy by changing the polarization of the THz beam and measuring the different nonlinear response. Our measurements thus far have yielded negative results, i.e., the gap looks isotropic. A possible explanation is that the quasiparticles formed by broken Cooper pairs scatter from one node to another in a time scale shorter than the THz pulse, thereby randomizing the effect of the THz polarization. While there is no doubt that the high intensity THz pulses cause the breaking of the Cooper pairs and induce a nonlinear response, it is yet unclear what the exact mechanism might be. Examination of the data has led us to believe that there might be two competing mechanisms at work: carrier acceleration by the THz field across the energy gap and direct photon absorption by the Cooper pairs.

Publications

1. E. Budiarto, J. Margolies, S. Jeong, J. Son, and J. Bokor, "High intensity THz pulses at 1 kHz repetition rate," IEEE J. Quantum Electron. vol. 32, pp. 1839-46, Oct. 1996.
2. J. Margolies, "Generation and propagation of high field Terahertz electromagnetic pulses" M. S. Thesis, University of California, Berkeley, 1996.

Students Supported

Joshua Cantrell

Shane Cantrell

Kevin Lascola

Jeff Margolies

Teh-Jiun Tung

Generation and Propagation of High Field Terahertz Electromagnetic Pulses

by Jeffrey Matthew Margolies

May 17, 1996

University of California at Berkeley

Department of
Electrical Engineering and Computer Sciences

Report for Master of Science
Plan II

Generation and Propagation of High Field Terahertz Electromagnetic Pulses

by Jeffrey Matthew Margolies

Research Project

Submitted to the department of Electrical Engineering and Computer Sciences, University of California at Berkeley, in partial satisfaction of the requirements for the degree of **Master of Science, Plan II**.

Approval for the Report and Comprehensive Examination:

Committee:

Professor J. Bokor
Research Advisor

5/16/96

(Date)

T.K. Gustaf

Professor T.K. Gustafson
Second Reader

5/16/96

(Date)

Acknowledgments

I would like to express my sincerest thanks to my research advisor, Professor Jeffrey Bokor, for his wisdom, encouragement, guidance, support, and patience throughout the course of this work. It was my privilege to work with Prof. Bokor from the moment he explained energy bands to the completion of my masters thesis. It has been my great privilege to be associated with Professor Bokor's ultrafast laser lab and semiconductor group.

I would like to thank all of my colleagues in Professor Bokor's research group for their support and useful interaction. I would especially like to mention Seongtae Jeong, and Joohiuk Son for their lengthy discussions, and invaluable help in the laboratory, and Troy Clear for his guidance in the Microfabrication Laboratory. But most of all, it was my great luck to work at length with Edward Budiarto, whose previous and continued work in this area and expert guidance has enabled me to produce the majority of the material contained within.

I would like to thank my friends outside of the EECS department for their support and encouragement. I would especially like to mention Eric Bone for the generous donation of his computer to write this report.

And last, but certainly not least, I am greatly indebted to my family for their emotional support, encouragement, and financial support for the first 23 years. From now on it really counts.

Table of Contents

I. Introduction

High power sub-single cycle electromagnetic pulses are useful tools for probing optical properties in various materials[1,2,3,4,5]. These pulses have frequencies and bandwidths ranging into the terahertz (THz) regime, allowing studies of material response at these frequencies where there are few good sources. Most of these studies utilize low power, small gap antennas. However, the radiated powers of large gap antennas are now reaching levels that allow the study of nonlinear effects. Specifically of interest, when peak electric fields of the THz pulse reach levels near 100kV/cm, the study of high field carrier dynamics in semiconductors is possible. In short channel MOSFETS, the velocity saturation regime starts altering device behavior when the electric field in the channel reaches these strengths. Therefore, it will be possible to use high field THz pulses to mimic high field regimes in bulk semiconductors without actually fabricating a MOSFET, and possibly effecting the physics involved.

THz generation by biased photoconducting antennas has been studied in depth by many groups[6]. The pulses are generated by placing a large bias across a semi-insulating (SI) semiconductor, like SI GaAs. The semiconductor is illuminated by 100fs laser pulse, generating a large number of free carriers in a short period of time, which are subsequently accelerated by the bias field. This acceleration of the carriers emits radiation in the form of a pulse, the shape of which is proportional to the time derivative of the current, as with a dipole radiator. The main lobe of the pulse has a width on the order of the laser pulse, so the transform, or spectrum, of the pulse will have frequency components ranging into the THz regime. Current efforts[7] to scale the THz energy to higher energy levels have concentrated on increasing bias levels, antenna sizes, and laser fluences. Pulse energies as high as 0.8μJ have been reported[8] at repetition rates of 10Hz by biasing a 3.5cm x 3.5cm GaAs antenna at 10.7kV/cm and illuminating at fluence saturation of 40μJ/cm^2. We report[9] the generation of 0.4μJ THz pulses at 1kHz repetition rate by biasing a 3cm x 4cm GaAs antenna at 10kV/cm at a fluence of 40μJ/cm^2.

Of primary importance in determining the electric field strengths obtained by focusing the radiation from the antennas is a greater understanding of the propagation behavior of THz beams. In Gaussian optics, there is a basic assumption of narrowband light. However, in our situation, the bandwidths are of the same order as the center frequency, so it is not immediately evident that the generally accepted values for diffraction and focusing of single wavelength light will be applicable.

In order to determine how the THz propagates from the antenna, the electric field in the antenna must first be known. The electric field profile of the antennas are studied using three methods. An electrooptic measurement technique is used to directly map the field across the antenna. A THz technique is used in which a small area of the antenna is irradiated with the laser pulse, and the resulting THz energy is measured. Finally a simulation is performed using the Laplace equation to compare with the measurements.

The propagation of THz beams is studied using the full broadband Huygen-Fresnel solution. From this solution, the electric field at any point in time and space can be determined from the electric field in the pupil. Using the electric field profiles above, general "rules of thumb" were obtained for diffraction from an aperture and focusing. It was found that the THz behaves much as a Gaussian beam, but with slightly different proportionality constants. These "rules of thumb" allow one to determine peak field strengths obtained at various places in an optical system to accurately specify experimental conditions.

Another topic of interest is how to scale the THz energies to higher levels. Currently, these antennas cannot be biased at any higher levels because of air breakdown across the gap. As seen in Paschen's curves[10], air breakdown is a function of the number of ionizing collisions that occur in the gap. The number of collisions is simply proportional to the number of molecules, so at a constant air pressure, as the gap size increases, the number of molecules increases and the breakdown field decreases. Therefore, since THz energy is

seen to go quadratically with bias field, this severely limits the amount of THz radiation possible. Also limiting the amount of THz energy generated is limited laser energy. For 10Hz operation, saturation levels of $40\mu J/cm^2$ have been observed, so laser energies of 1mJ can illuminate an area of $25cm^2$ without loss of efficiency. However, at 1kHz repetition rates, saturation levels are approximately $150\mu J/cm^2$, making operation at $40\mu J/cm^2$ inefficient, and limiting area to around $7cm^2$. An in depth study of the behavior of THz radiation on fluence, bias, and gap size was performed to completely understand the situation.

The results of the studies show that for limited laser energy, and therefore limited antenna size, the best possible solution is to go to large areas and small gaps. Therefore the possibility of using antenna arrays was investigated. The propagation of small and large gap arrays was simulated and compared to experiment. Also, possible geometries for small gap arrays were investigated. A large gap array was built and performed as simulated, verifying the accuracy of the simulations. However, attempts at building small gap antennas were unsuccessful. Possible reasons for this are discussed.

Finally, included in the Appendix are the basic core of the propagation simulations used in section III, along with an in depth process flow of the small gap aluminum absorber antenna array fabrication.

II. Electric Field Measurements

To better understand how the Terahertz (THz) beam propagates, it is important to know the pupil function. The pupil function is the electric field across the antenna gap, so measurements were performed on electric field verses position in the gap. This was measured in two manners. First, with an electrooptic (EO) technique which directly measured the field across the gap, and secondly, by measuring the THz energy generated as a function of location in the gap, and inferring the bias field profile. From previous studies,[11] it has been observed that the electric field is highly asymmetric across the gap, with large enhancement near the anode caused by a trap enhanced electric field. It was shown that this effect was gap dependent, with maximum enhancement at a gap size of 80μm, so it was not evident what the electric field profile might be for centimeter sized gaps.

The EO measurement technique used, outlined in Budiarto et. al.[12], utilizes the GaAs antenna as the EO medium. Following the discussion of Yariv and Yeh[13], GaAs is a $\bar{4}3m$ cubic crystal, with a symmetric, equal valued EO tensor given by,

$$r_{jk} = \begin{pmatrix} 0 & 0 & 0 \\ 0 & 0 & 0 \\ 0 & 0 & 0 \\ r_{41} & 0 & 0 \\ 0 & r_{41} & 0 \\ 0 & 0 & r_{41} \end{pmatrix}, \tag{1}$$

where $r_{41}=1.62\times10^{-12}$m/V. For arbitrary bias field, this leads to an index ellipsoid given by:

$$1 = \frac{\left(x^2 + y^2 + z^2\right)}{n_0^2} + 2r_{41}\left(E_x yz + E_y zx + E_z xy\right). \tag{2}$$

For a (100) GaAs wafer, there is no orientation of bias field that will lead to a transverse EO effect[14], which due to the geometry of our antennas is the desired effect. Therefore, we used a nonstandard (110) SI GaAs wafer as the EO medium, which did not have any effect on the THz output but allowed the measurement of a transverse EO effect. A (110)

wafer has a major flat also along a (110) plane, specifically $(\bar{1}10)$, but due to the symmetry of GaAs, this plane is indistinguishable from a (110). Therefore, if we apply a transverse electric field perpendicular to the major flat, or along a (110) direction of $E_x = E_y = E/\sqrt{2}$, and E_z=0, the index ellipsoid becomes,

$$1 = \frac{\left(x^2 + y^2 + z^2\right)}{n_0^2} + \sqrt{2}Er_{41}\left(yz + zx\right). \tag{3}$$

To solve this problem we need to solve the eigenvalue equation,

$$\begin{pmatrix} 1/n_0^2 & 0 & r_{41}E/\sqrt{2} \\ 0 & 1/n_0^2 & r_{41}E/\sqrt{2} \\ r_{41}E/\sqrt{2} & r_{41}E/\sqrt{2} & 1/n_0^2 \end{pmatrix} \vec{V} = \frac{1}{n'^2}\vec{V} \tag{4}$$

Where the eigenvector, $\vec{V}$, gives the new principle axes, and the eigenvalue n' gives the new principle index of refraction. The normalized solution of the problem is easily shown to be,

$$\vec{V} = \begin{pmatrix} x' \\ y' \\ z' \end{pmatrix} = \begin{pmatrix} 1/2 & 1/2 & -1/\sqrt{2} \\ 1/2 & 1/2 & 1/\sqrt{2} \\ 1/\sqrt{2} & -1/\sqrt{2} & 0 \end{pmatrix} \begin{pmatrix} x \\ y \\ z \end{pmatrix} \tag{5}$$

$$\begin{aligned} n_{x'} &= n_0 + \frac{n_0^3 r_{41} E}{2} \\ n_{y'} &= n_0 - \frac{n_0^3 r_{41} E}{2} \\ n_{z'} &= n_0 \end{aligned} \tag{6}$$

Therefore, linearly polarized light will pick up a maximum polarization rotation of $\Gamma = \pi V/V_\pi$ when oriented 45° in between x' and y', i.e. the (110) direction, where

$$V_\pi = \frac{\lambda d}{2Ln_0^3 r_{41}} \tag{7}$$

is the voltage required to delay the phase by a half wave, V is the applied voltage across the gap, d is the gap spacing, L is the thickness of the wafer, and n_0 is the ordinary

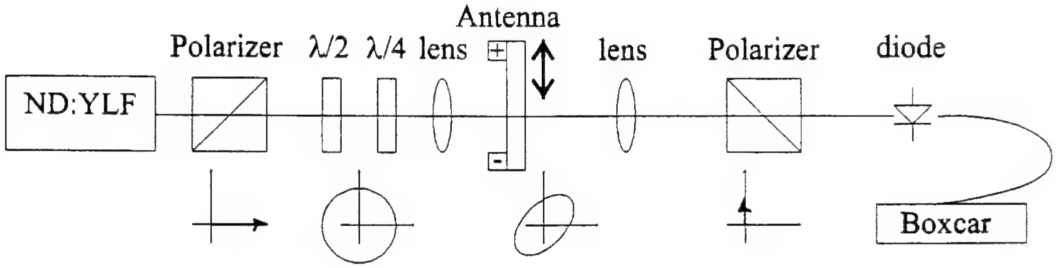

Figure 2.1. Experimental setup used to measure electric field dependent rotation of polarization.

refractive index of GaAs. Putting in typical numbers for GaAs, V_π/d=139kV/cm. Typically, we operate at only 10kV/cm, so additional phase rotation is needed to operate in the linear regime. This is achieved by utilizing a quarter waveplate prior to the GaAs wafer.

The experimental setup is shown in figure 2.1. A CW Nd:YLF laser is passed through a series of a polarizer, half wave and quarter wave plate to produce circularly polarized

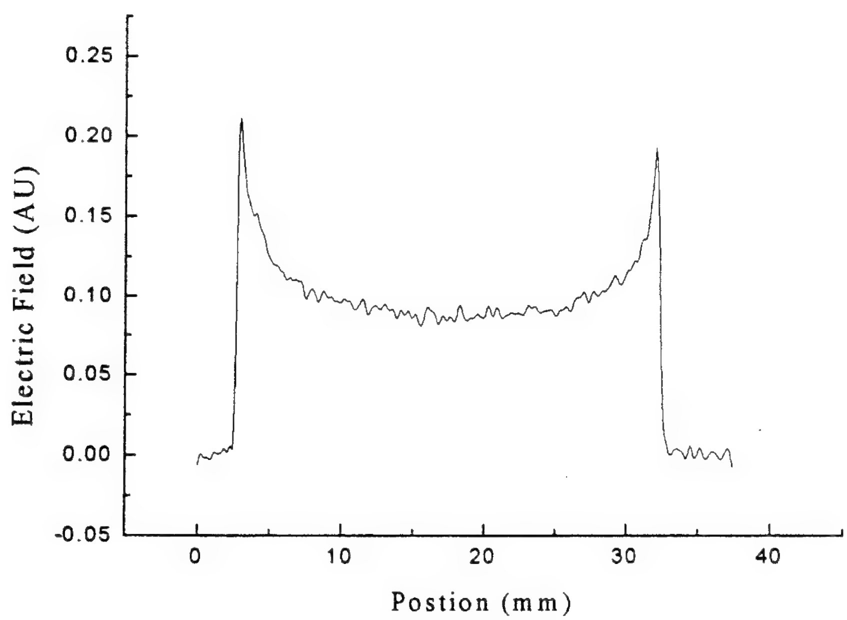

Figure 2.2. Plot of Electric field vs. position in the gap as measured by the electrooptic effect.

light, which places the beam in the linear response regime. It is then focused to a 100μm spot with a lens onto the surface of the (110) GaAs wafer. The wafer has evaporated aluminum electrodes 3cm wide and 3cm apart. It is biased using a homemade voltage pulser capable of applying 45kV in a 2μsec pulse at 1kHz. The wafer is mounted on a translation stage so that the position of the focused beam can be scanned across the gap. After passing through the wafer and picking up additional phase retardation, Γ, it is recollimated and passed through a second polarizer, oriented along the (110) direction as suggested above, which analyzes the phase shift. This is focused onto a large area photodiode to minimize any beam shift caused by scanning the wafer. The detected signal is sent through a boxcar averager which is triggered by the voltage pulser, and analyzed with a computer.

The results of this experiment are shown in figure 2.2. This is a plot of signal on the photodiode as a function of location in the gap. Since we are in the linear regime, this is proportional to the electric field across the antenna. As can be seen, the electric field

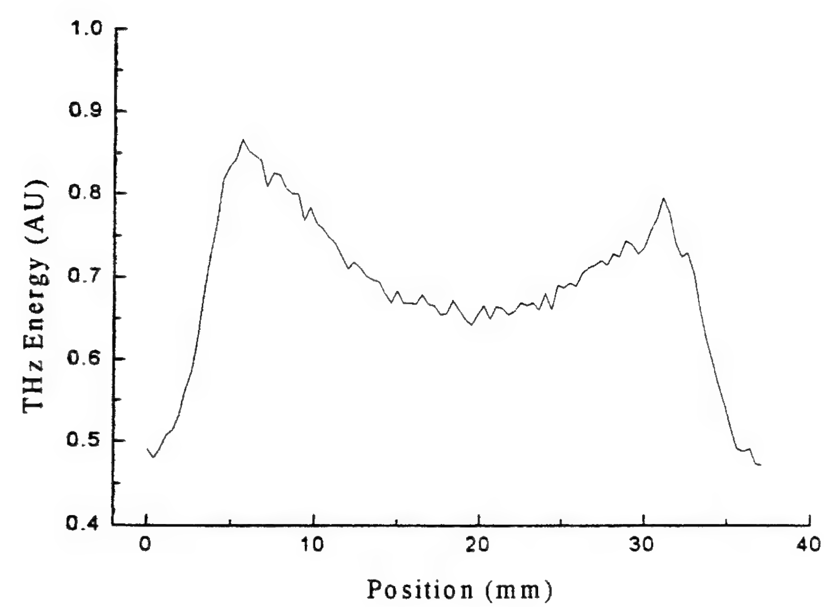

Figure 2.3. THz energy as a function of position in the gap measured by exciting only a 1mm area of 3cm antenna with laser, and scanning the laser spot across the gap.

strength at the electrodes is more than twice that in the center. This enhancement can be attributed solely to geometrical effects caused by the thin electrodes on top of the wafer. This shape is similar to what occurs at the edge of a parallel plate capacitor, except that in our case, all we have is the edge. No trap enhancement as observed by Grischkowsky in reference 11 is seen for these large gaps.

An alternate experiment was performed in order to verify the results of the EO measurements. In this situation, THz was generated across a 3cm gap antenna by illuminating only a 1mm diameter area of the wafer with the Ti:Sapphire laser beam and scanning the illuminating spot across the front of the antenna. The radiated THz energy was then measured as a function of position in the gap. As seen in figure 2.3, a plot of THz energy as a function of position of the pinhole, the general crown shape is again observed. In this situation, the peak to valley ratio is approximately the same, but the sharpness of the peak is much less. This can be attributed to a convolution effect with the

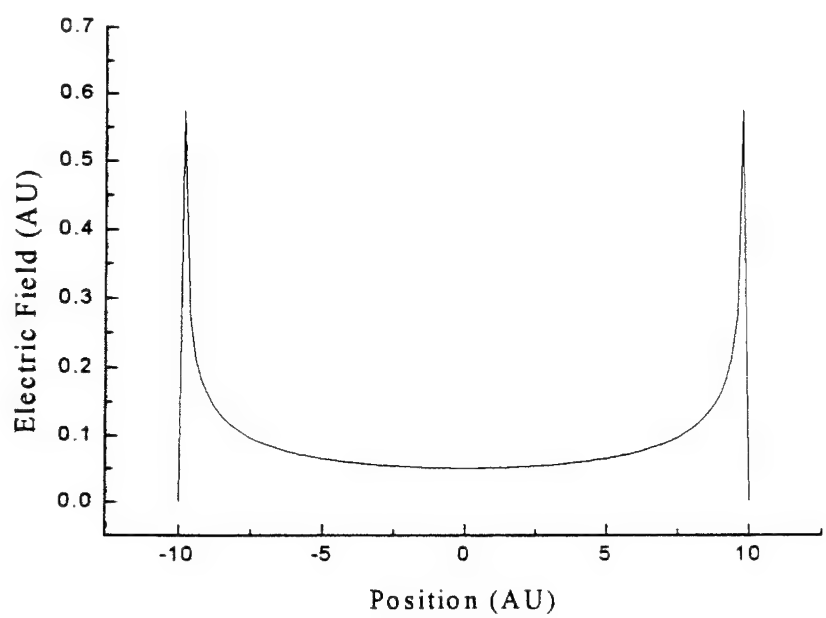

Figure 2.4. Theoretical result for electric field across dielectric with two thin electrodes on top. Field and distance scale to arbitrary values.

large laser spot.

A numerical simulation was performed to model the above measurements. This simulation assumed that the GaAs wafer is a dielectric, dielectric constant ε=13.3, with two thin electrodes on top of the wafer. The Laplace equation was solved to determine the scalar potential at all points in space, and from this, the electric field across the gap was obtained by taking the negative gradient of the potential in the gap. The results of this calculation is shown in figure 2.4. Here electric field as a function of location in the gap is shown. As can be seen, the electric field at the edges of the gap are greatly enhanced do to the geometry of the antenna. It should be noted that although it appears that there is much more enhancement in the simulation than in the experimental results, the peaks in the simulation are very narrow. Therefore, it is possible that the experimental results have more enhancement than is evident in figures 2.2 and 2.3, but that the spatial averaging caused by the finite spot sizes used washes out the larger peaks seen in the simulation.

Using this knowledge of the magnitude of the electric field across the gap, we are now able to use this information as a pupil function in a study of how THz pulses propagate in free space, and how they are focused by a lens. Armed with these two tools, one is able to calculate the behavior of most optical systems necessary in experiment.

III. Terahertz Propagation

In order to study the propagation of the THz beam, the full Huygen-Fresnel broadband solution was implemented[15]. This solution states that the electric field at any point after an aperture can be determined by integrating the time derivative of the electric field, evaluated at a time retarded by the propagation from the pupil to the observation point, multiplied by an angular factor, divided by the distance traveled.

$$u(P_0,t) = \int_{\Sigma} \frac{\cos(\hat{n},\vec{r}_{01})}{2\pi c|\vec{r}_{01}|} \frac{d}{dt}\left[u\left(P_1, t - \frac{\vec{r}_{01}}{c}\right)\right] ds \tag{8}$$

The geometry of this equation is shown in figure 3.1, where $u(P_0,t)$ is the electric field at point P_0, the angular term is the cosine of the angle between $\mathbf{r_{01}}$ and $\mathbf{n}$, the unit normal, Σ, is the aperture, and $\mathbf{r_{01}}$ is the vector from $\mathbf{P_1}$ to $\mathbf{P_0}$. This solution is valid after only a few wavelengths, or within a few millimeters for THz frequencies.

The simulations performed using this full Huygen-Fresnel formalism were done on a workstation using C code written specifically for this problem. The main body of the simulation, shown in Appendix A, determines the intensity at some point a distance from the aperture by applying eqn.(8) and performing a time average over a time duration long

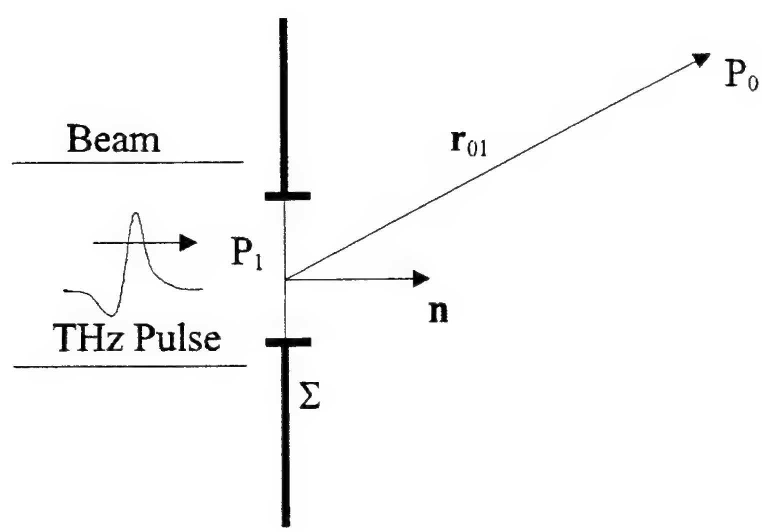

Figure 3.1. Geometry of Equation 3.1. A THz beam incident on an aperture Σ. Electric field at P_0 is obtained from the field at P_1.

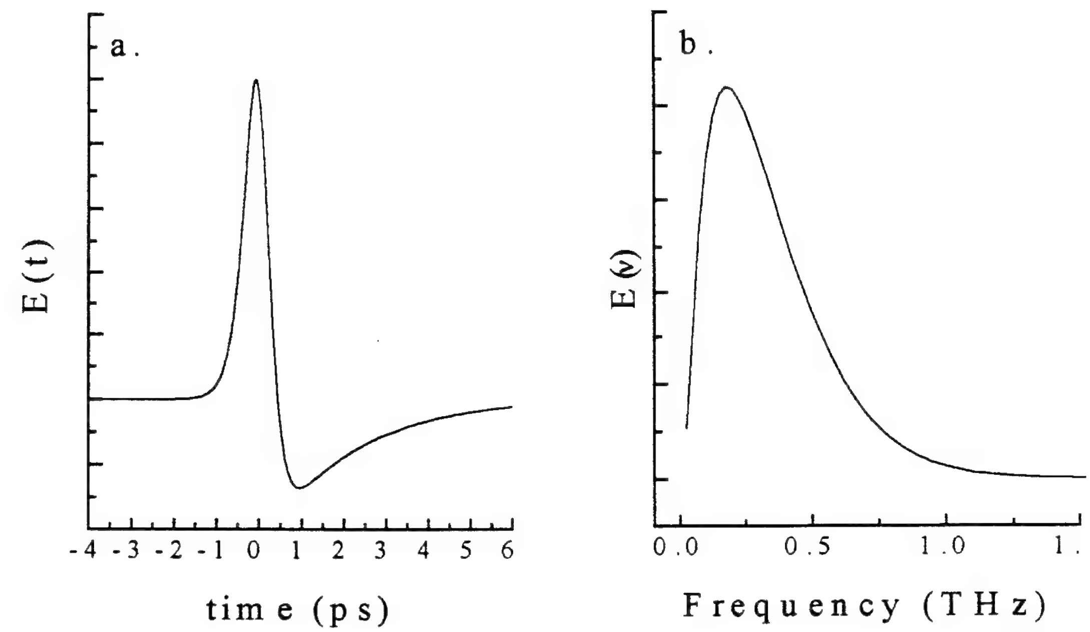

Figure 3.2. (a) THz pulse used in the full Huygen-Fresnel propagation simulations. The vertical axis is electric field, and the horizontal is time in picoseconds. (b) Magnitude of the electric field spectrum plotted vs. frequency. The majority of the spectrum is contained between DC and 1THz, with a mean value of 337GHz.

compared to the THz pulse and the relative path lengths in the problem. Variations of this main code were used to determine intensity profiles and propagation behavior.

The THz pulse, shown in cartoon fashion in figure 3.1, is shown along with the magnitude of the frequency spectrum in figure 3.2. This pulse is an analytical solution to the theoretical model for THz pulse generation[16,17]. It is the time derivative of the convolution of the laser pulse (assumed hyperbolic secant squared) and the exponential carrier decay. For the pulse of figure 3.2a, a laser pulsewidth of 200fs and carrier lifetime of 2ps were assumed. As can be seen, it is very similar to the observed THz pulses in reference 9, with a pulsewidth around 500fs, and the typical sub-single cycle shape. The magnitude of the spectrum, shown in figure 3.2b has frequency components ranging from DC up to one THz, with a mean frequency of 337GHz, corresponding to a mean wavelength of 900μm.

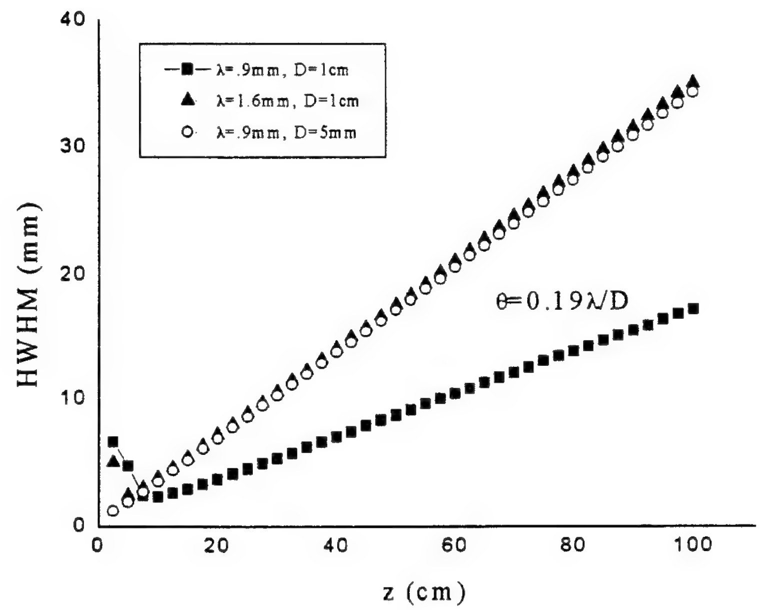

Figure 3.3. Divergence of THz beam. HWHM, or beam waist as a function of distance, z, from the aperture. Shown for two different aperture widths, 5mm and 1cm, and two mean wavelengths of .9mm and 1.6mm for 1cm aperture.

Also incorporated in this simulation is the fact that the diffracting aperture of interest during propagation is generally the antenna itself. Therefore, for simulations in the x direction, or across the gap, the electric field profile in the diffracting pupil, Σ, is actually the profile obtained in section II. The results of figure 2.4 are incorporated into the first group of simulations to most accurately represent the problem at hand.

The first problem investigated was propagation in free space away from the antenna. Figure 3.3 is a plot of HWHM, or the distance from the axis where the intensity falls to half the on-axis value, as a function of distance from the antenna for three different situations. The solid squares show divergence from a 1cm width aperture for the THz pulse shown in figure 3.2a. The open circles show divergence for a 5mm aperture for the same pulse. As can be seen, for half the aperture width, the divergence angle has doubled. The solid triangles show divergence from a 1cm aperture for a different THz pulse generated using a 400fs laser pulse, and having a mean wavelength of 1.6mm. As can be

seen, this diverges at approximately twice the angle of the shorter wavelength pulse through the same aperture. Therefore, we arrive at a wavelength and aperture width dependent divergence angle of $\theta=0.19\lambda/D$, where λ is the mean wavelength and D is the aperture width. The functional form of this is similar to that obtained for Gaussian beams[18], where $\theta=\lambda/\pi D$.

Next investigated was the question of how far from the aperture the beam must propagate before it is in the farfield, or Fraunhofer, regime. The farfield pattern is obtained by making two approximations to the full H-F solution. The first is that the distance from the observation point to the aperture is sufficiently large so that first, the $1/r_{01}$ dependence can be approximated as a 1/z dependence and taken out of the integral, and second, the cosine term becomes unity. The second approximation is that the r_{01} in the phase is first expanded with a binomial expansion, and then the terms quadratic in the pupil are dropped.

$$u(x,t)=\frac{1}{2\pi cz}\int_{\Sigma}\frac{d}{dt}\left[u\left(\xi,t-\frac{z\left(1+\frac{x^2-2x\xi}{2z^2}\right)}{c}\right)\right]d\xi, \tag{9}$$

Where ξ is the pupil coordinate and x is the image coordinate, and the problem has been reduced to one dimension. Once these approximations are made in eqn.(9), the results are compared with eqn.(8). The distance at which they agree satisfactorily (within 5%) was defined to be the minimum distance at which the farfield approximation is valid.

The results of the farfield calculations are shown in figure 3.4. Here, z_{ff} is plotted as a function of the aperture width. For large aperture widths, greater than 7mm, z_{ff} is seen to increase quadratically with D, $z_{ff}=2.6D^2/\lambda$. For values of D below this, z_{ff} saturates. Qualitatively, as the aperture width approaches the size of a few wavelengths, the diffraction pattern from the aperture approaches that of a simple dipole radiator, and the diffraction angle is independent of aperture size. When this occurs, it is no longer the phase approximation that is limiting the validity of the Fraunhofer approximation, but the

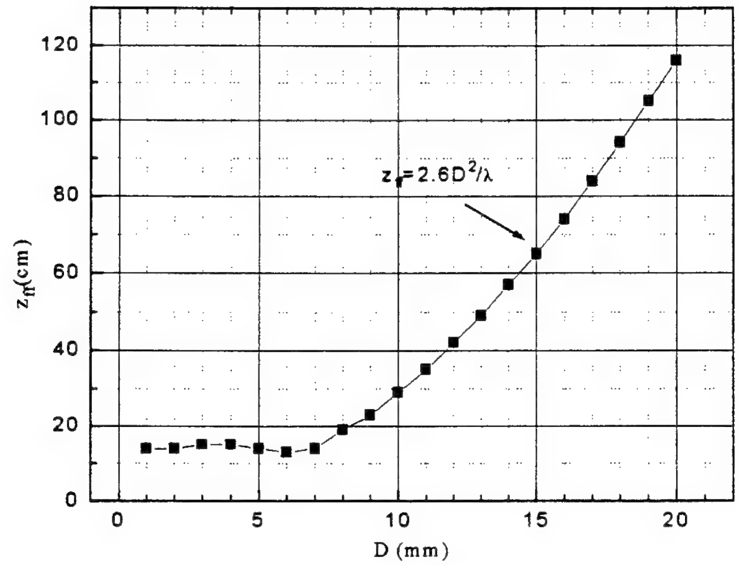

Figure 3.4. Minimum distance for which Fraunhofer approximation is valid as a function of aperture width. Quadratic dependence for apertures larger than 7mm, virtually constant for smaller apertures.

approximation in the denominator. This approximation was basically a small angle approximation, and will not be effected in this small aperture regime since the angles are no longer changing. The large aperture result is similar to that of circular apertures, where $z_{ff} >> D^2/\lambda$ is the typical "rule of thumb".

Of major importance in understanding the propagation of THz beam is a greater comprehension of how this broadband radiation focuses. In order to accomplish this, a quadratic phase was added across the aperture to mimic a lens. This is the same as placing a lens, focal length f, immediately after the antenna. In eqn.(10), this quadratic phase appears as an additional time delay in the electric field that is a function of the pupil coordinate, ξ.

$$u(P_0,t) = \int_{\Sigma} \frac{\cos(\hat{n},\bar{r}_{01})}{2\pi c|\bar{r}_{01}|} \frac{d}{dt}\left[u\left(P_1, t - \frac{\bar{r}_{01}}{c} + \frac{\xi^2}{2cf}\right)\right] d\xi \tag{10}$$

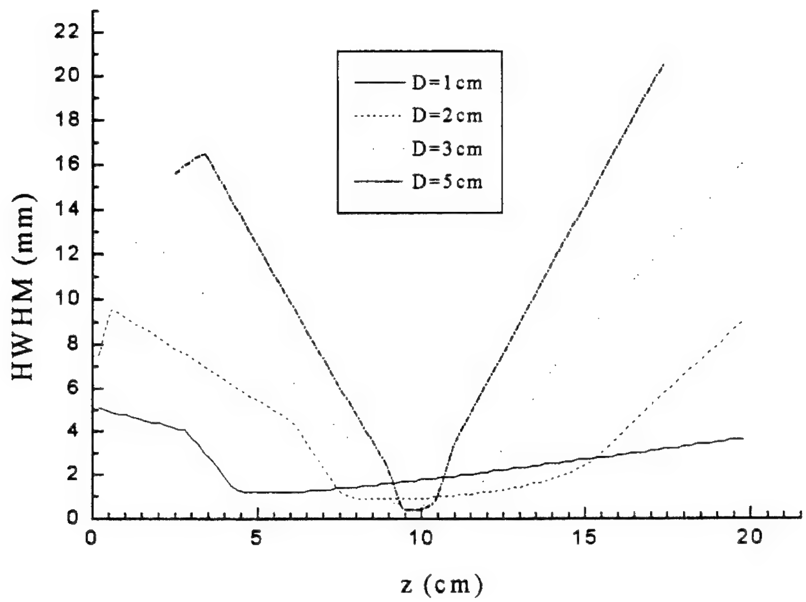

Figure 3.5. HWHM, or beam waist, as a function of distance z from the lens, focal length *f*, for various aperture widths, D. Seen here is the *f*/# dependent focal shift, spot size, and depth of focus.

Scans of the focal region were performed to determine how typical geometries behave. Figure 3.5 shows the results of a series of such scans. HWHM of the beam is plotted verses distance from the aperture of a 10cm focal length lens. The various curves are for different aperture widths, or various *f*/#'s, where a lens *f*/# is given by the ratio of the focal length to the aperture width. A low *f*/# lens denotes a tightly focusing geometry, while a weak lens has a large *f*/#. As can be seen, for the *f*/2 lens, or D=5cm, the beam focuses to a tight spot for a short distance (small depth of focus), and leaves the focal region at the same angle that it arrived. However, as the *f*/# increases, the focal region becomes asymmetric, and the focal point actually shifts to the left, or in towards the aperture. This focal shift in turn alters the effective *f*/# of the lens, which effects the beam waist and depth of focus.

Focal shift for Gaussian beams at optical frequencies is generally only on the order of tens of microns, so the effect on *f*/# is only a fraction of a percent. However, for THz beams,

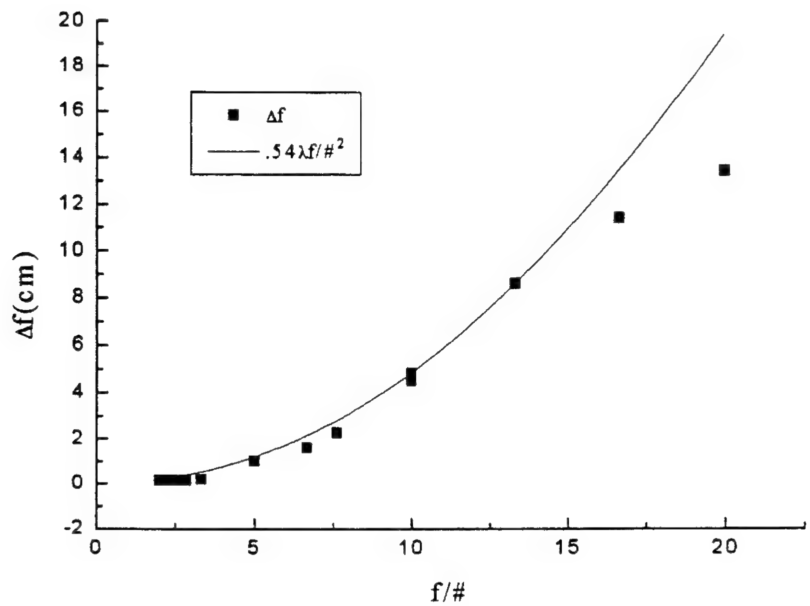

Figure 3.6. Focal shift as a function of geometrical f/# for THz beams.

the focal shift for an *f*/5 optic is approximately a centimeter, which can have a significant effect on the *f*/#. For Gaussian beams, the actual focal point is given by[19],

$$f_{new} = \frac{f}{1 + \left(\frac{f\lambda}{\pi w^2}\right)^2} \tag{11}$$

where f_{new} is the shifted focal length, f is the geometrical focus given by the lens makers formula, and w is the Gaussian beam waist at the lens. For the THz simulations, figure 3.6 shows the focal shift as a function of geometrical *f*/#. The focal shift, f-f_{new}, is shown to increase quadratically as a function of geometrical *f*/# for values below approximately *f*/15, and to saturate above this value. The saturation occurs for high *f*/# because at these small lens powers, the lens is unable to counter the effect of diffraction, and the position of the minimum spot size approaches the aperture. The form of the focal shift appears to be, $f - f_{new} = \Delta f = 0.54\lambda f/\#^2$, which leads to an f_{new} of,

$$f_{new} = f\left(1 - \frac{0.54\lambda f}{D^2}\right). \tag{12}$$

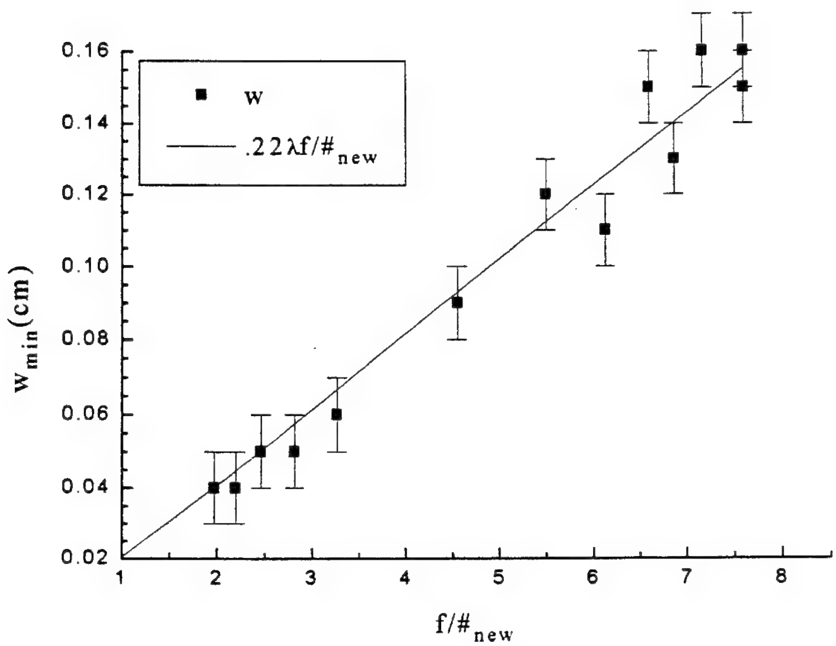

Figure 3.7. Minimum spot size as a function of shifted f_{new}. Linear dependence within error bars.

It is simple to show that eqn. (12) will approach eqn. (11) for wavelengths short compared to f and D.

Figure 3.7 shows the minimum spot size as a function of f_{new}. It is seen to increase linearly with f_{new}. The error bars in figure 3.7 are a result of the finite discretization used in the simulation. The best linear fit to the data is $w_{min}=0.23\lambda f/\#_{new}$, where w_{min} is the minimum spot size, located at f_{new}, and $f/\#_{new}=f_{new}/D$. Therefore, the full expression for w_{min} is given by,

$$w_{\min} = w(f_{new}) = 0.23\lambda \frac{f}{D}\left(1 - \frac{0.54\lambda f}{D^2}\right) \tag{13}$$

This linear dependence on $f/\#$ is similar to that obtained by circular apertures, as determined by the Rayleigh criterion, where $w_{min}=0.61\lambda f/\#$.

The depth of focus, z_0, define as the full width of the focal region for which the beam waist is less than $\sqrt{2}w_{\min}$, also behaves as expected once the shifted focus is taken into

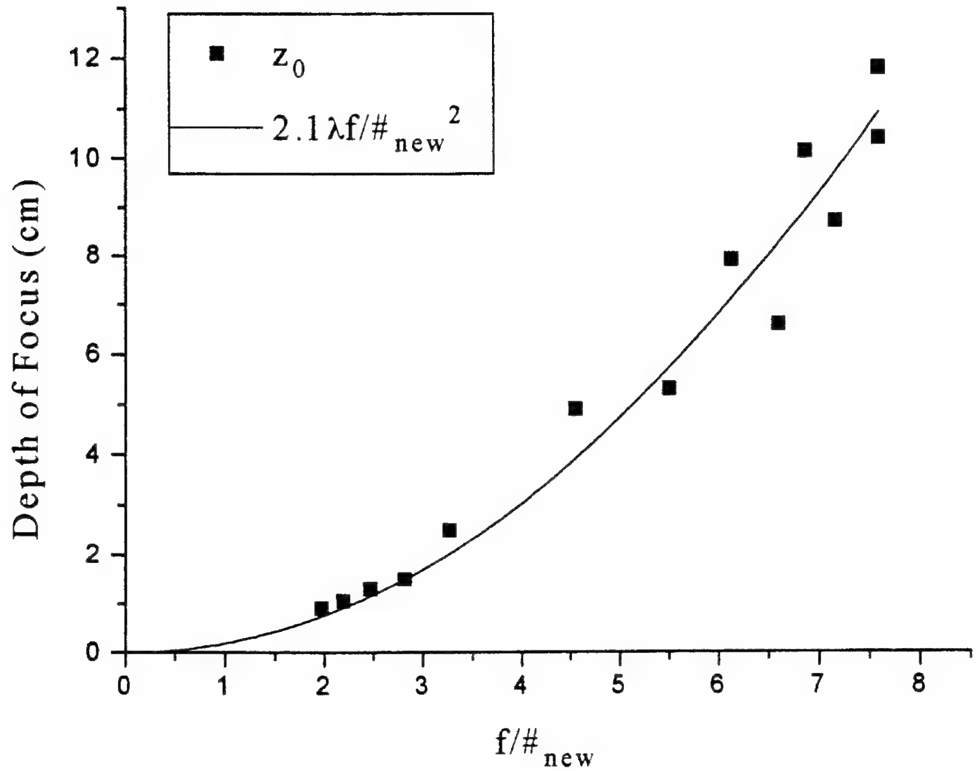

Figure 3.8. Depth of focus as a function of $f/\#_{new}$. Quadratic dependence similar to that of narrowband circular apertures.

account. Again from circular apertures, we expect that z_0 will increase quadratically with $f/\#$, as $z_0=2.44\lambda f/\#^2$. Figure 3.8 shows this quadratic dependence when plotted against $f/\#_{new}$, with the curvature given by a proportionality constant of 2.1. Therefore, the THz value of z_0 is given by $z_0=2.1\lambda f/\#_{new}^{2}$, or

$$z_0 = 2.1\lambda\left(\frac{f}{D}\right)^2\left(1-\frac{0.54\lambda f}{D^2}\right)^2 \tag{14}$$

One last set of simulations was performed to determine the focusing and divergence properties of the beam in the dimension parallel to the electrodes (y direction). In the y direction, there should be approximately no variation in electric field across the gap, so the

	Crown profile (x direction)	Rect profile (y direction)
Divergence angle	$\theta=0.19\lambda/D$	$\theta=0.25\lambda/D$
Farfield validity	$z_{ff}=2.6D^2/\lambda$	$z_{ff}=2.6D^2/\lambda$
Focal shift	$f-f_{new}=\Delta f=0.54\lambda f/\#^2$	$f-f_{new}=\Delta f=0.54\lambda f/\#^2$
Focal Length	$f_{new}=f\left(1-\frac{0.54\lambda f}{D^2}\right)$	$f_{new}=f\left(1-\frac{0.54\lambda f}{D^2}\right)$
Spot Size	$w_{min}=0.23\lambda f/\#_{new}$	$w_{min}=0.27\lambda f/\#_{new}$
Depth of Focus	$z_0=2.1\lambda f/\#_{new}^2$	$z_0=2.5\lambda f/\#_{new}^2$

Table 1. Summary of THz propagation behavior. X direction, parallel to the applied bias includes the crown profile of figure 2.4. Y direction, parallel to the antenna electrodes, has a rect function profile.

aperture was modeled as a simple rect function. The results looked qualitatively the same, and the numbers were as follows.

The divergence was found to be greater, at $0.25\lambda/D$. The minimum farfield distance was the same, as was the shifted focal length, therefore there is no built in astigmatism. The minimum spot size is larger at, $w_{min}=0.27\lambda f/\#_{new}$. And finally, the depth of focus was also larger, at $2.5\lambda f/\#_{new}^2$. Therefore, since the antennas are square, the propagation of these antennas is an

inherently separable problem, and these results, along with the previous results in the x direction, specify the appearance of the beam at any point in the farfield or in the focal region. It should be noted that since the beam generated in the y behaves effectively as a smaller beam (greater divergence, spot size, and depth of focus), then it is beneficial to make this dimension larger to decrease the diffraction from this direction and match the propagation in the two dimensions. This is in fact done, as the large aperture antennas are 3cm gaps, but 4cm wide. The results of these simulations are summarized in Table 1.

To determine how valid the results of the simulations were, they were compared to experimental results. A 3cm gap antenna was placed immediately in front of an off-axis

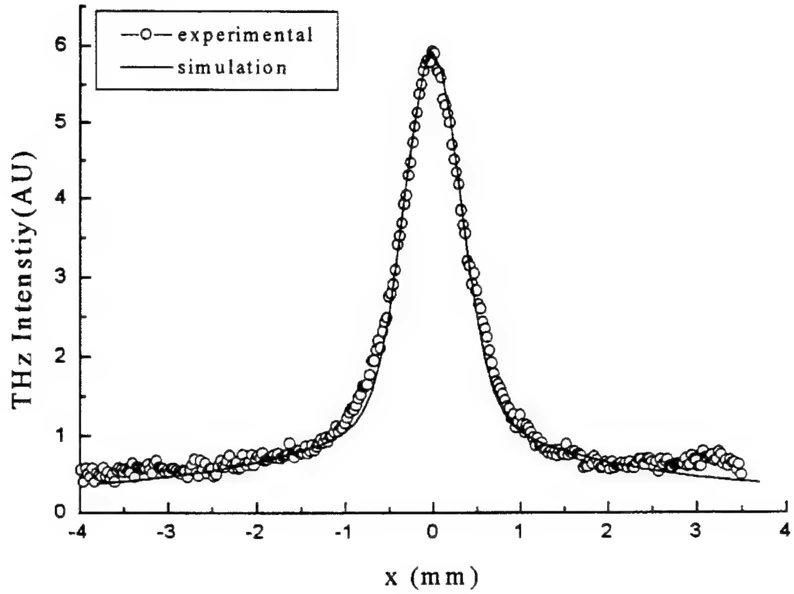

Figure 3.9. Focal scans of 3cm THz beam for a 2.5" focal length parabola. Open circles are experimental results, line is simulation result.

2.5" focal length parabola. A 600μm pinhole was scanned across the THz focus at various z positions. The results of the scan which achieved the minimum spot size is shown as open circles in figure 3.9. As can be seen, the fwhm of the experimental data is approximately 1mm. Also shown in the figure is the result of the above simulations. The simulation was convolved with a 600μm rect function to mimic the experimental setup. The fwhm of the experimental and simulated results agree very well at a value of 1mm. The width before convolution of the simulation was 875μm. There is slight deviation from experimental in the wings, but it should be noted that the experimental setup is actually a 2D problem, while the simulation was only in 1D.

With this simulation tool, and the above formulas for THz beam propagation and focusing, we are now able to look at methods for increasing the THz energy. One method that immediately presents itself is reducing the *f*/#'s to achieve smaller focal spots, and therefore higher peak intensities and fields. This is limited by manufacturing since *f*/#'s

much below 2 are highly impractical. Therefore, methods for increasing the THz energy need to be investigated. This is the subject of the next section.

IV. Increasing THz Energy.

The current experimental setup used to generate high power THz beams consists of a 3cm gap antenna, 4cm wide, on SI GaAs. The bias is provided by a homemade high voltage pulse generator which provides 2μs pulses with peak voltages as high as 45kV at 1kHz repetition rate. The laser is a Clark-MXR regenerative amplifier system, capable of generating 1mJ energy pulses at 1kHz repetition rate, with pulsewidths of 100fs. The laser is typically operated at 600μJ energies with pulsewidths of 200fs.

At a 3cm gap size, air breaks down at approximately 15kV/cm, and with the laser on, aiding in the ionization of air, the air breaks down at 10kV/cm. This data is shown in figure 4.1 for various sized gaps. This plot shows the breakdown voltage of air while generating THz pulses as a function of gap sizes. The data for large gaps, from 0.5mm to 9 mm, is shown on the right half of the plot. The antennas are two 5mm x 2mm

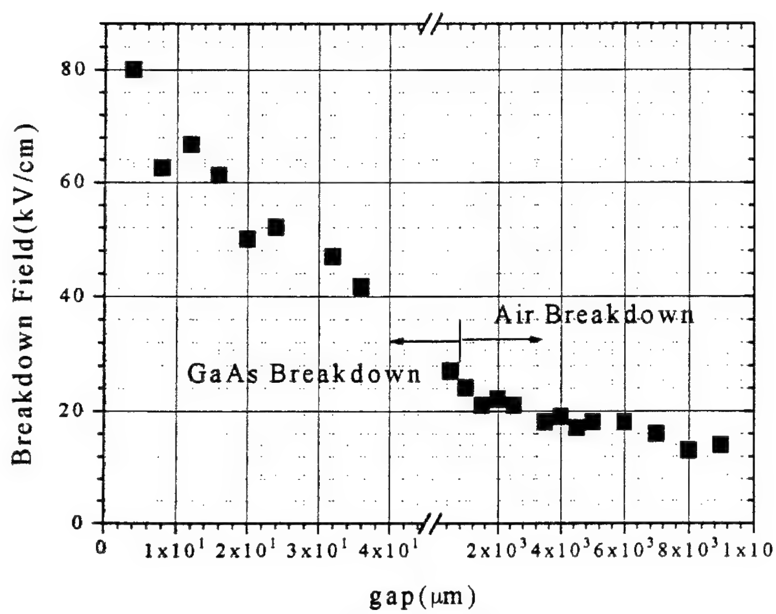

Figure 4.1. Breakdown electric field across two Ti-Au lines for various gap separations. For gaps 1mm and larger, air breakdown is the limiting breakdown mechanism, while for smaller that 1mm, the mechanism is GaAs breakdown.

evaporated Ti-Au contacts (3000A of gold on top of a 300A layer of titanium used for adhesion) separated by the gap size. As can be seen, as the gap size increases, the breakdown field decreases, leading to less efficient THz antennas. For 9mm gaps, the breakdown occurred at 14kV/cm, while the 1mm gap antenna broke down at 24kV/cm.

Also shown in figure 4.1 are the results of measurements for small gap antennas. These antennas are 4mm x 10μm Ti-Au lines. For gap sizes below 1mm, air breakdown is no longer the mechanism for device failure, but rather avalanche breakdown in the SI GaAs itself dominates. For the small gaps, the breakdown was measured on an IV curve tracer, and was defined as the voltage at which the current was 50μA. As can be seen, for a 40μm gap, the breakdown field occurred at 42kV/cm and ranged all the way up to 80kV/cm for a 4μm gap.

THz energy is seen to increase quadratically with bias field, therefore increasing the bias has a large effect on the amount of THz energy generated. It is also seen to increase

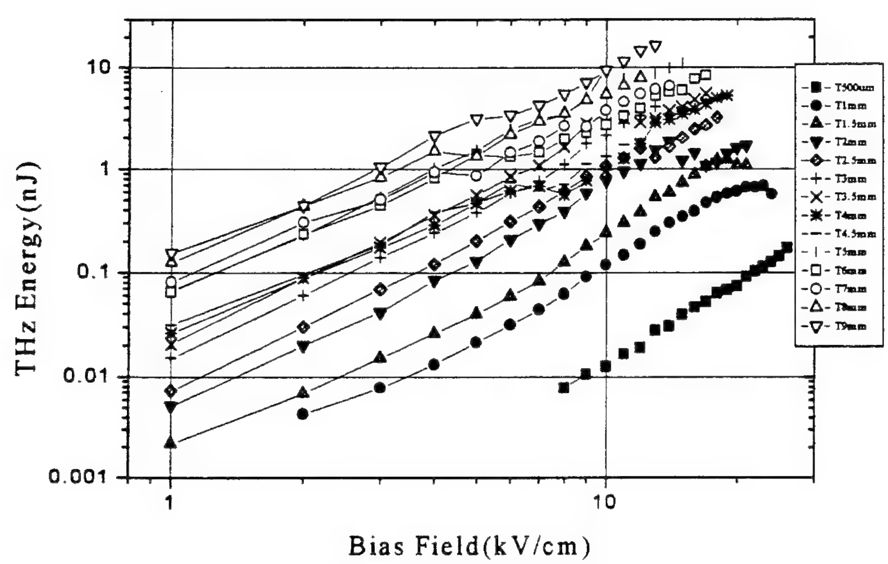

Figure 4.2. THz energy as a function of bias electric field across various gap sizes. THz increases quadratically (slope 2) with bias field and linearly with gap size.

linearly with antenna area. Figure 4.2 shows results for studies on the amount of THz generated as function of bias electric field for various gap sizes. The measurements were performed on the same 0.5mm to 9mm antennas as the large gaps above. As the bias field was increased, the THz energy was measured as emitted by the back side of the wafer by a bolometer. The bolometer was placed approximately 1cm behind the antenna to minimize the effects of different coupling efficiencies for different gap sizes. The absolute energy was calibrated by comparing the bolometer output to the output of a pyroelectric detector which was calibrated to the laser energy. As expected, the emitted THz energy increases quadratically with bias field (slope of 2 on the log-log plot). Also seen is the fact that the smaller gaps are able to be biased to higher electric fields. However, the higher biases are not enough to overcome the loss of antenna area, and at no point does a smaller antenna emit more energy than a larger one.

Figure 4.3 is a plot taken from figure 4.2, showing the THz energy as a function of gap

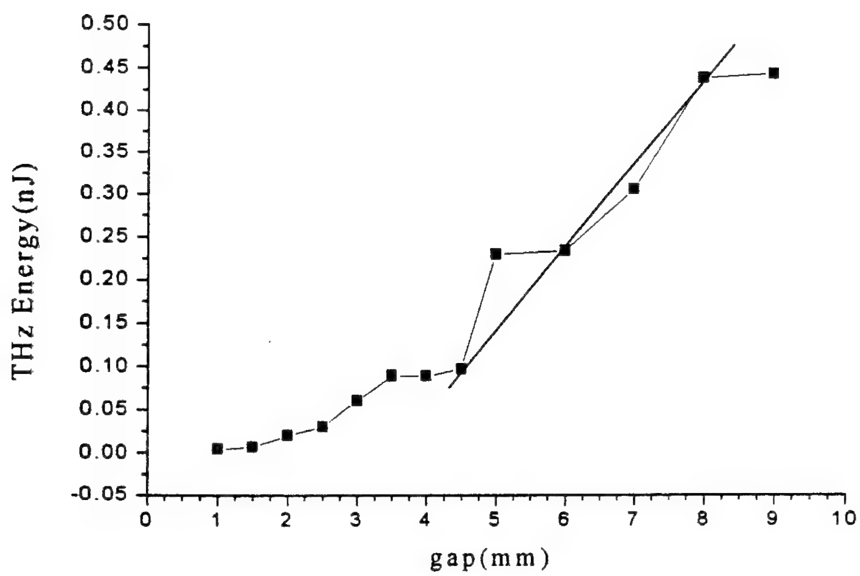

Figure 4.3. THz energy as a function of gap size for bias of 2kV/cm. Linear dependence for gaps larger than 4.5mm.

size for one particular bias field of 2kV/cm. As can be seen, the emitted THz energy increases approximately linearly for gap sizes above 4.5mm. This means that for these gaps, the increase in THz is changing linearly with area. For the smaller gaps, the amount of THz generated becomes sublinear. This is attributed to the fact that the divergence of the THz beam for these small gaps is very large, leading to a reduced amount of THz energy coupling out of the wafer and into the bolometer.

This suggests that the best way to increase the THz energy is to continue to increase the gap sizes above 3cm. However, this does not take into account the influence of limited laser energy. As stated above, the laser is generally operated at approximately 600μJ energy. Therefore, for our 3cm x 4cm antenna, the maximum laser fluence achievable is 50μJ/cm^2. For 10HZ repetition rate, it is generally accepted that THz output energy saturates with a laser fluence of 40μJ/cm^2.[20] However, as reported by Budiarto et. al.[21], at 1kHz, this saturation level is much higher. Figure 4.4 shows data for THz energy as a function of laser fluence for several different gap sizes between 0.5mm and 2.5mm. The

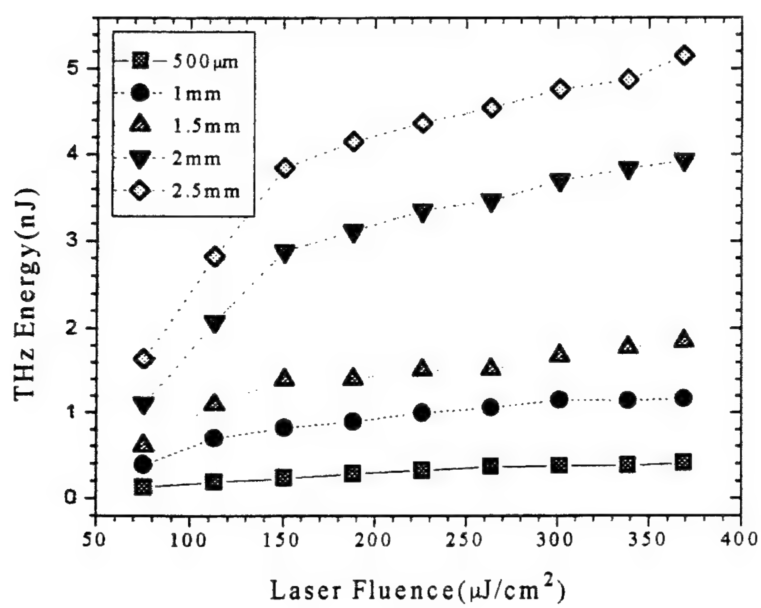

Figure 4.4. THz energy as a function of laser fluence for various gap sizes. Clear saturation is observed at fluences of 150μJ/cm^2.

fluence was varied by placing a waveplate-polarizer combination in the beam, and rotating the waveplate to vary the transmission through the polarizer. As can be seen, there is a clear region for all gaps where the THz energy increases approximately linearly with laser fluence, until 150μJ/cm^2, at which point the THz energy saturates. This saturation level was seen to be the same for all gaps up to 9mm. Therefore, at fluences of 50μJ/cm^2, we are not in the saturation regime, and any increase in area causes a similar decrease in fluence, resulting in no net increase in THz energy generated. There is, however, an increase in numerical aperture (decrease in *f/#*), which causes tighter focusing of the beam, and therefore higher peak fields at the focus even though there is no more THz generated. There is a price to pay with larger and larger gaps, however, as the air breakdown continues to decrease, and the voltages, already in the 30kV range, get larger and larger, requiring extreme safety precautions.

To sum up the preceding section, the data suggests that to increase the THz energy at the focus of a parabola, the antenna area should be large, the fluence high, the repetition rate high, and yet the gap small. Therefore, the natural solution to this problem is to go to arrays of antennas. This is the subject of the next section.

V. THz Antenna Arrays.

As stated in the above section, the clear direction leading to increased THz energy without further scaling of the antenna areas is the use of antenna arrays. There are many possible array schemes to choose from, as well as many possible gap sizes. For medium gap sizes (hundreds of microns), schemes of cascading voltages have been fabricated[22], whereby several adjacent gaps add up in phase to produce one large beam. However, as the number of gaps increase, the complexity of the biasing scheme increases, and the voltage requirements increase rapidly. The simplest imaginable scheme, in which only one bias voltage is required, is an interdigitated finger structure, as shown in figure 5.1. The problem with this structure is that each adjacent gap is radiating a THz beam which is precisely 180° out of phase with the next. Every other field is pointing in the opposite direction. Therefore, in the farfield, they will all cancel with each other, barring any edge effects, and the device will not radiate. Therefore a scheme must be obtained to somehow block the radiation emitted from every other gap, or block every other gap from radiating.

First, using the simulation tool described in section III, the various antenna arrays were modeled to verify that, indeed, an array of small gaps with alternating sign would not radiate into the farfield, and also to see if an array with every other gap blocked would radiate. Figure 5.2 shows the results of these calculations for 5mm arrays of 25μm gaps. The pupil function used was a periodic rect function, with a period of 25μm, multiplied by

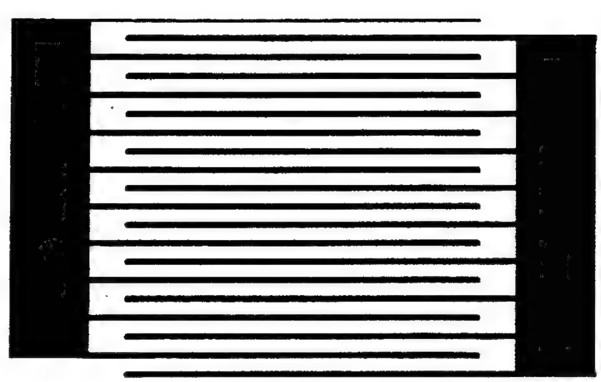

Figure 5.1. Possible THz antenna array with interdigitated finger structure.

a large rect function with a width of 5mm. The periodic function had a value of one or zero for the array with every other gap blocked, and a value of plus or minus one for the array without every other one blocked. The influence of electric field within the gap, as given in section II was neglected for these simulations.

Figure 5.2a shows the results of a simple 5mm aperture focused by an *f*/3 lens (i.e. in the farfield). The maximum intensity on axis (x=0) is normalized to one, and the full width of the focal region was found to be 0.8mm. Figure 5.2b shows the results of the antenna with every other gap blocked. As can be seen, the width of the focal region is the same, since the numerical aperture is unchanged, however the peak height is one quarter that of the large aperture antenna. This means that the antenna array, biased to the same field, would only emit a quarter of the radiation. However, recall figure 4.1. A gap of 5mm will break down at a field of 18kV/cm, while a 25μm gap will withstand a field over 50kV/cm. Therefore, after the biased is doubled to counteract the loss in area, every gain in bias is a gain in energy. As the areas are scaled to larger values, and the gap sizes are reduced, the

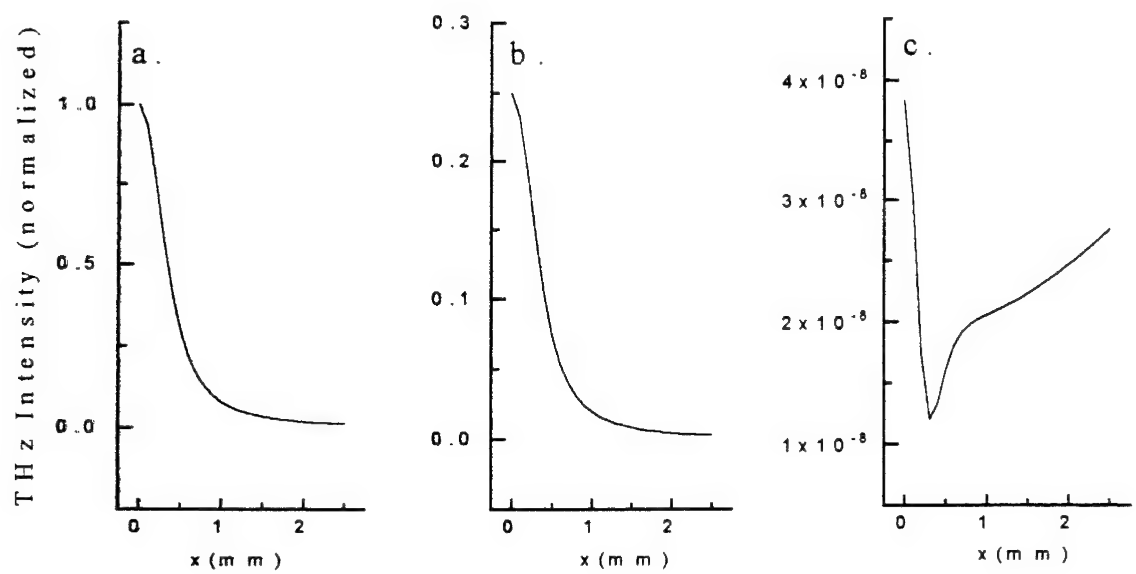

Figure 5.2. Plots of intensity vs. position from center of beam out (symmetric about axis) at the focus of *f*/3 lens for 3 different antenna types. a. 5mm gap antenna. b. 5mm array of 25μm gaps with every other gap blocked. c. 5mm array of 25μm gaps with every other gap opposite sign.

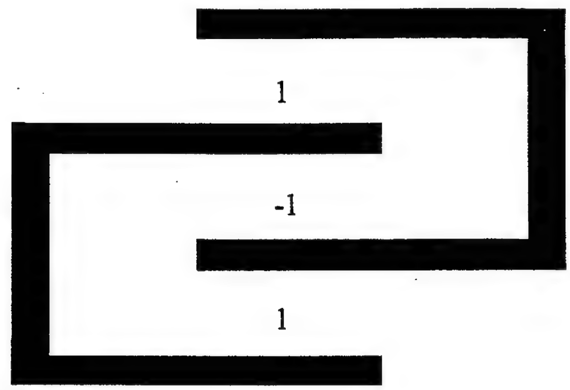

Figure 5.3. Large gap antenna array used to experimentally verify interdigitated finger concept. Numbers denote direction of bias field. Each gap is 5mm.

relative gains are enhanced.

Finally, figure 5.2c shows that, indeed, an antenna with alternating fields will not radiate. This is similar to the discussion by Goodman,[23] where a source with a coherence area much smaller than a wavelength will not propagate. All of the random phases will add up to zero in the farfield. In our situation, instead of having random phases adding up to zero on average, we have carefully designed phases which add up to zero. Thus we are left with a simple, non radiating, evanescent wave.

To further check that these simulation results were valid experimentally, simulations were done for large gap arrays. The three array structures investigated were first, a 5mm gap, second, three adjacent 5mm gaps, with the one on the inside having a bias direction in the negative direction, and the two on the outside having positive biases, and third, the second antenna with the middle section blocked. The three situations are denoted as 010, 1-11, and 101 respectively. Experimentally, this situation was achieved with a simple 3 element interdigitated finger array shown in figure 5.3. By blocking the two outside gaps, an 010 antenna was generated. By blocking the middle gap, a 101 was achieved, and by not blocking any, a 1-11 was generated. Blocking of various gaps was done by placing an adhesive dielectric absorber in the gap to block the laser radiation from exciting this section of the antenna. The end regions were also masked off to reduce edge effects.

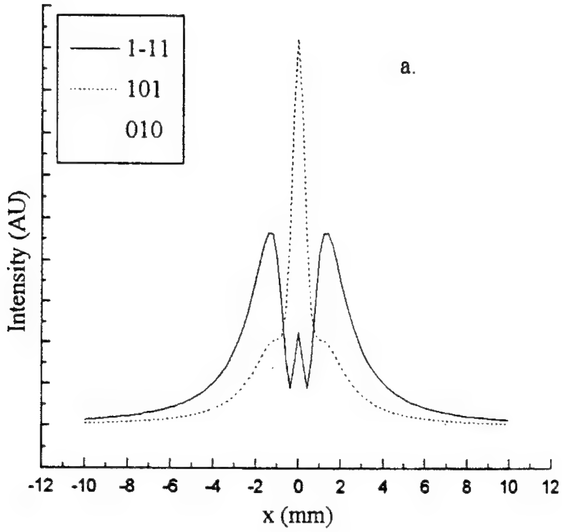

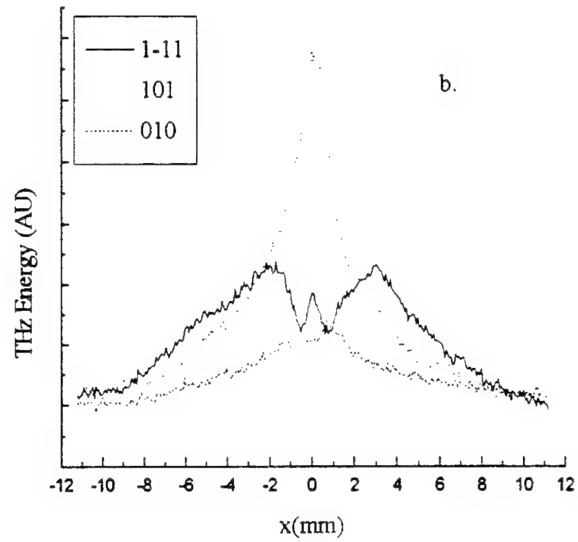

Figure 5.4. THz intensity at the focus of 2.5" focal length parabola as a function of position, x, in the focus. a. Simulations of 3 different 5mm element antenna array schemes. b. Experimental results for the same three antennas.

The simulation results for the focusing of these three antennas by a 2.5" focal length parabola are shown in figure 5.4a. The solid line is for the 1-11 antenna. It shows 3 distinct peaks. The middle peak comes from the two outside elements adding in phase, and the inside element subtracting in phase, resulting in an on axis height of 1. The two outer peaks correspond to the positive peak from the outside elements adding in phase with the second, negative (but switched due to the sign of the field), peak of the inner element. Near the axis, at the focus of a lens, the electric field is very close to bipolar, so the combination leads to a height of 2.

Figure 5.4b shows the same basic shape for the experimentally measured 1-11 in the solid line. These measurements were done on the above mentioned 1-11 array, with the end regions masked off. The antenna was placed directly in front of a 2.5" focal length parabola, and the energy was scanned at the focus. The scanning aperture was a 700μm slit. A slit was used as opposed to a pinhole to increase signal to noise, and should not

cause any loss of information due to the 1 dimensional nature of the problem. As can be seen, it has the same 3 peaks, slightly washed out due to convolution with the slit.

Also shown in figure 5.4a are the results of the 010 and 101 simulations. The 010, shown in dotted line form, has a half width of approximately 3mm, and a height of 1. The 101 has a height 4 times higher, and half the width, from the two adding coherently on axis. The 101 also shows a fairly extensive wing structure, from the individual pulses propagating essentially without interference (due to the finite pulsewidths). This is exactly what is shown in the experimental scans of figure 5.4b. The 101 has 4 times the peak energy on axis, and half the width. Therefore, if we were to use this antenna to increase the THz output, we should compare it to a 1cm gap antenna. The effective area of generation is the same, so for the same bias field (twice the voltage), the two emit the same energy. The array, having a larger extent, will focus tighter, but there is a loss of laser fluence, which will reduce the generated THz energy. Also, the array, having a smaller gap, will be able to withstand a larger bias field.

These results are promising in that they show that, in fact, the simulation results for large gaps are valid, and therefore, we assume that the small gap simulations are also valid. Therefore, in the future, small gap antenna arrays can be fabricated in which the gains from increased bias fields more than offset the losses in antenna area. Furthermore, the use of LT GaAs materials, in which the breakdown electric fields are enhanced by factors of 5 to 10 over SI GaAs, could lead to even more gains in output THz. One possible isolation scheme is shown in figure 5.5. This device uses an aluminum mask deposited on top of a dielectric isolation layer to selectively block the laser from exciting every other gap. The interdigitated fingers are a 3000A layer of gold on top of a 300A layer of titanium used for adhesion. The pattern is formed by patterning photoresist (PR), evaporating the metal, and liftoff. The silicon nitride layer is deposited using a plasma chemical vapor deposition, and is as thick as can be allowed without cracking from stress. The aluminum mask is formed with a second PR and liftoff step. Finally, a third mask step is used to open up contacts through the nitride.

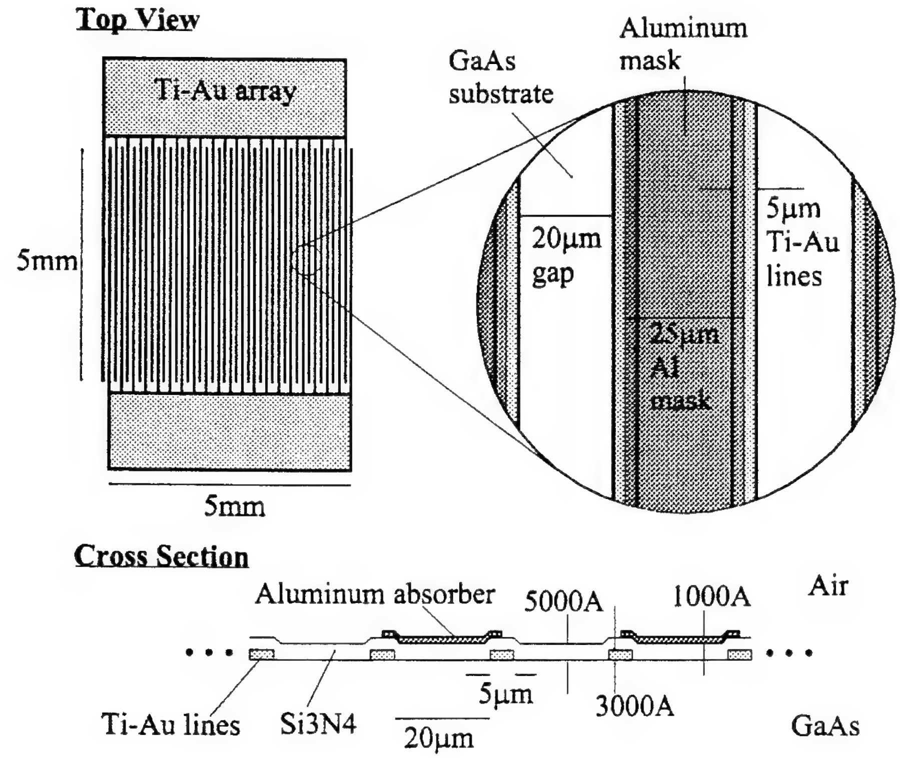

Figure 5.5. Possible antenna array device that uses an aluminum absorber mask to prevent the laser from exciting every other gap. 5mm array of 20mm gaps, shown without Al absorber at top left, with Al absorber in top right blow-up, and in cross section at the bottom.

An in depth process flow is shown in Appendix 2. This antenna array was actually fabricated, but due possibly to fabrication errors, did not work. Two different antennas were fabricated that were able to withstand a voltage (i.e. were not shorted due to fabrication errors). The first emitted THz, but the energies were 100 times smaller than expected. The second device had an

alignment error in the second mask stage, such that 5% of the gap that was supposed to be blocked was exposed. If the field across the gap were constant, this would not be a problem. However, as seen in section II, the fields at the edges are greatly enhanced, and in fact, the majority of the THz generation comes from these regions. Therefore, the effect of the misalignment was to block one of the good peaks, and to expose one of the bad ones, resulting in exactly the situation we are trying to avoid by using the mask in the first place, alternating plus and minus fields. Furthermore, for the first device, it is now

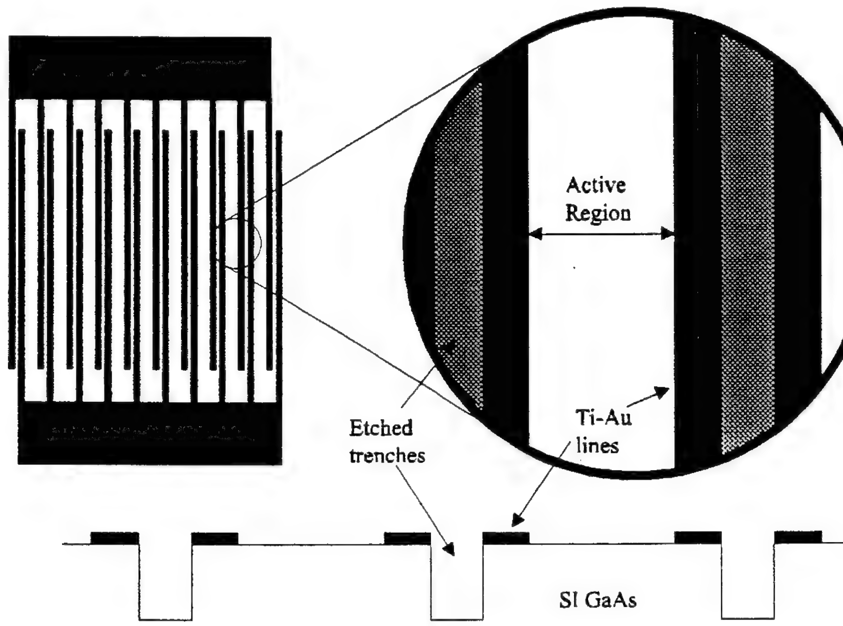

Figure 5.6. Mesa isolation scheme in which the field is isolated in every other gap by etching trenches deep enough to reduce the electric field at the bottom of the trench significantly.

evident that any light that manages to get into the blocked gap, mostly from diffraction, will tend to cancel out the radiated field, and this is exacerbated by the edge enhancement effects which are even worse in the presence of the isolation mask. Therefore, wider aluminum absorbers to reduce the amount of light diffracting into the blocked gap, combined with possibly thicker mask layers might aid in reducing this effect.

Another promising isolation scheme is a mesa isolation scheme, or field isolation technique. This scheme, depicted in figure 5.6, isolates every other gap by etching trenches into the GaAs. If the trenches are deep enough to reduce the electric fields at the bottom of the gap sufficiently, then only every other gap will radiate THz. Simulations similar to those that generated figure 2.4 suggest that in order to reduce the field in the middle of the trench to 10% of the field in the middle of the gap at the surface, the depth of the trench must be 1.25 times deeper than the active gap if the two gaps are the same width. Therefore, if the gap is 10μm wide, the trench must be 12.5μm wide. If an asymmetric geometry is used, as suggested by figure 5.6, then the trench depth must be increased. For instance, if the trench width is reduced to 5mm, then the depth must be

25μm, leading to an aspect ratio of 5 to 1, which may be difficult to achieve etching GaAs using a reactive ion etcher. This requirement of 10% reduction in field at the middle of the trench compared to the middle of the gap might be too stringent, however. Since the fields are so peaked at the edges, the majority of the THz is emitted in this region, and shallower trenches may be sufficient.

VI. Conclusions

In order to better understand the propagation of THz beams from large gap antennas, several studies were carried out. First, the electric field in the antenna was mapped as a function of position across the gap using three methods. The first was a direct measurement of the electric field using the electrooptic effect in (110) GaAs. The second was an indirect method whereby the THz emitted as a function of location in the gap was measured, giving us a map of the electric field squared in the gap. Third, the electric field was obtained through simulation by solving the Laplace equation for a similar geometry. It was found that all three results showed heightened fields at the electrodes, and this was attributed to the geometry of the electrodes. The electrodes exhibit edge effects similar to those seen at the edge of a parallel plate capacitor.

This electric field mapping was subsequently used to generate THz propagation "rules of thumb" by solving the full broadband Huygen-Fresnel integral. It was found that the beams diverge proportional to λ/D. The farfield approximation was valid for distances proportional to D^2/λ. There is an f/# dependent focal shift that effects the beam waist and depth of focus. Consequently, the values of the beam waist and depth of focus vary as expected when the focal shift is taken into account.

Next, an in depth study was performed on how the THz antennas vary with gap size. Measurements on electric field breakdown show that for millimeter sized antennas, the breakdown mechanism is avalanche breakdown in the air, while for gaps smaller than a millimeter, there is breakdown in the GaAs. The breakdown fields are significantly higher for gaps in the ten micron range than for gaps in the centimeter range. It was also found that the saturation fluence was independent of gap size, and occurred at a value of $150\mu J/cm^2$, leading to the conclusion that the most efficient antenna areas for this laser is $6.7cm^2$ for typical laser energies of 1mJ.

Finally, using the information of section 4, it was shown that the most promising way to increase the THz energy without upgrading lasers is to go to a small gap antenna array scheme. The simulation of array propagation was verified for large gaps, and a large gap, three element, antenna array was successfully patterned and tested. To conclude, possible isolation methods for fabricating small gap antenna arrays were discussed, with particular attention on how to eliminate the THz generated from opposing gaps.

Appendix A

```
/*************************************************************************
 * Program Huygen_Fresnel.c determines the intensity at some point x and z from an      *
 * aperture. X is the distance from the optical axis, z is the distance from the aperture.   *
 * The formula used is the full Huygen Fresnel broadband solution, as given by Goodman.*
 * The main body is a simple time loop which calculates the electric field over a long     *
 * period of time, and averages the magnitude squared to obtain the intensity. The THz  *
 * pulse comes from the analytical time derivative of the convolution of the laser pulse,    *
 * width t1, and the carrier lifetime, t2, The time derivative of this is used in the program. *
 * The pupil function can in general be anything. For an array (shown) it is alternating    *
 * ones and zeros, or ones and minus ones. For a single gap, the electric field profile      *
 * should come from a data file to mimic the edge enhancement effects                        *
*************************************************************************
/*************************************************************************
*                                                                                          *
*                        Written by Jeff Margolies 3/6/96                                  *
*                                                                                          *
*************************************************************************/
/*************************************************************************
*                                                                                          *
*   Units are all in picoseconds for time, and 100's of microns for distance. Note, for   *
*    these units the speed of light is 3.0                                                 *
*                                                                                          *
*************************************************************************/

#include<stdio.h>
#include<math.h>

#define t1 0.2              /*Laser Pulsewidth 200fs                          */
#define t2 2.0              /* Decay time 2ps                                 */
#define Num 500             /* Number of time points to average over          */
#define Dt 0.04             /*Time step 40fs, total averaging time ± 20ps     */
#define Pi 3.1416
#define Mult Dt*1.3281E-15  /*multiply by .5 ε0 c to make Joules/m^2          */
#define C 3.0               /*speed of light in units of 100um/ps             */
#define Width 300.0         /*Total aperture width 3cm                        */
#define L .25               /*single element of array width 25μm              */
#define Dx 1.0              /*Integration step size in pupil                  */
#define f 500.0             /*focal length of lens = 5cm                      */


double dwdt() ;             /* Analytical time derivative of THz waveform     */
```

```
double diff();              /* Huygen-Fresnel Integral                              */
double pupil();             /* Pupil function. Magnitude of electric field in pupil */
int sgn();                  /* sgn function, returns sign of the argument           */

main()
{
double  fi, fj, time, efield;
double  x, z, intensity;
int  j, k;
FILE  *fint;

        x=0.0;                              /*set x and z values*/
        z=f;                                /*unit 100um*/

        fint=fopen("intensity.out","w");    /* output data file */

        intensity=0.0;                      /* Intensity initialized to zero */

        for( j = -Num ; j <= Num ; j++ ){   /*loop for time*/

                time = ((double)j)*Dt+sqrt(z*z+x*x)/C ;  /* Time, centered so that t=0 is
                time it *
                                                  *takes radiation from center of         *
                                                  * aperture to travel to the  observation*
                                                  * point                                 */

                efield=diff(x,z,time);                   /* call HF function */
                intensity=intensity+efield*efield;;   /*add up electric field at each time*/

        } /*end time loop*/

        intensity=intensity*Mult;                 /* Convert to SI units of Fluence (J/m^2)
*/
        fprintf(fint,"%E  %E  %E \n",x,z,intensity);     /* output intensity in data file */
        fclose (fint);
} /*end of main body of program */

/***********************************************************************
*                                                                      *
* dwdt returns the analytical time derivative of the THz pulse. The input arguments  *
*  are x, z, t,  where x is the distance from the axis, z is the distance from the antenna,  *
* and t is the time.                                                   *
***********************************************************************/
```

```
double dwdt(t)
double t;
{
double tmp1,tmp2;

        tmp1=1+exp(t/t1);
        tmp2=-8*exp(t/t1)*((1/t1-1/t2)*exp(t/t1-t/t2)-exp(2*t/t1-t/t2)/t2);
        tmp2=tmp2/tmp1+4*t1*((1/t1-t/t2)*(1/t1-1/t2)*exp(t/t1-t/t2)-(2/t1-
                1/t2)*exp(2*t/t1-t/t2)/t2);
        tmp2=tmp2/tmp1/tmp1;

        return tmp2;
}

/**********************************************************************
*                                                                     *
* diff(x, z, t) returns the value of the Huygen-Fresnel Integral at position x,z, time t     *
*                                                                     *
**********************************************************************/

double diff(x,z,t)
double x,z,t;
{
double amp, xi,r01;
int i, W;

        tmp=0.0;

        W=(Width/Dx);       /* Width of aperture in units of Dx */

        for(i=-W/2; i<=W/2 ; i++) {             /* loop across the pupil                 */
                xi=((double)i)*Dx;              /*variable of lateral dimension in the slit */
                r01=sqrt(z*z+(x-xi)*(x-xi));    /*distance from obs to source             */
                amp=amp+pupil(xi)*(z/2/Pi/C/r01/r01)*dwdt(t-r01/C+xi*xi/2/C/f)*Dx;

                                /* This particular version includes quadratic time delay for *
                                 * simulating a lens.  To remove this, send f to infinity       */
        }

        return(amp);
}
```

```
/***********************************************************************
*                                                                      *
* Pupil(x) returns the magnitude of the electric field in the aperture. The argument, x,  *
*  is the location in the pupil.  Shown are 3 cases. The first is a constant pupil, the   *
second can be to generate alternating 1's and zero's, with period L, and the third        *
generates alternating 1's and -1's.                                                       *
*                                                                      *
***********************************************************************/

double pupil(x)
double x;
{
double amp;

        amp=1.0;

/*      amp=.5-.5*sgn(cos(Pi*x/L));          */  /*Alternating 1 and 0*/

/*      amp=sgn(cos(Pi*x/L));                */  /*this will be alternating +-1*/

        return(amp);

}

/***********************************************************************
*                                                                      *
* sgn(x) is the sign function, returns the sign of the argument (±1)   *
*                                                                      *
***********************************************************************/

int sgn(x)
double x;
        {

        if (x>=0) return 1; else return -1;

        }
```

Appendix B

Process flow for fabricating absorber isolation array (figure 5.5).

I. Clean Wafer
   A. Acetone rinse
   B. Isopropyl rinse
   C. DI rinse
   D. Dry nitrogen
II. Pattern Photoresist, mask 1
   A. Pre-bake wafer for 20 min. at 120C (evaporates any water)
   B. HMDS bubbler 5 min. (prepare surface so resist sticks)
   C. Spin 1.5μm layer of positive resist
      1. Microposit 1400-31 positive resist
      2. 6000rpm for 30 sec.
   D. Bake 8 min. in 90C oven. (pre-bake)
   E. Let cool on heat sink
   F. Chlorobenzene dip 5 min. (hardens surface for good liftoff overhang)
   G. Bake 15 min in 90C oven
   H. Expose pattern with Quintel 1:1 contact printer
      1. Align wafer to mask
      2. Expose 5 seconds in vacuum contact mode
   I. Develop in Microposit developer 1:1 DI 45 sec. (do not over-develop too much or walls will collapse)
   J. DI rinse 30 sec. in beaker. (Careful of overhangs, be gentle)
   K. Dry nitrogen (At this point you should see good overhangs with optical microscope)
III. Evaporate Ti-Au in Veeco
   A. HCl:DI 1:4 20 sec. (Removes native oxide from rinse step)
   B. Use titanium granules and 12" of gold wire
   C. Use 2 separate .005 tungsten boats (must use the thin boats to keep from burning resist)
   D. Pump down to $5x10^{-7}$
   E. Evaporate 300A Ti at 160amps at 20A/sec (adhesion layer)
   F. Let chamber pump back down to $5x10^{-7}$
   G. Evaporate 3000A Au at 140amps at 40A/sec
IV. Lift-off
   A. Soak in Acetone for several hours.
   B. Repeat cleaning, Step I.
V. Nitride deposition in Technics A.
   A. Etch chamber with CF_4 plasma, (if organics present, run O_2 plasma)
      1. 10 minutes at 300mT CF_4, RF power of 150W
   B. Deposit 4000A Si_3N_4

1. Put wafer at 5 o'clock, middle of hot plate, along with Si test wafer
2. Set hot plate to 300C
3. SiH_4 flow at 10sccm
4. NH_3 flow at 90sccm, pressure should be 580mT
5. N_2 balance to 800mT
6. RF power 30W
7. Rate will be 100A/min

VI. Repeat Photoresist procedure (II) with mask 2
   A. Align mask using alignment marks and array
   B. Make sure mask centered well

VII. Evaporate aluminum in Veeco
   A. HCl:DI 1:4 20 sec.
   B. Use aluminum pellets in thin tungsten boat (1 pellet = 1000A)
   C. Evaporate at least 1000A at 140amps at 20A/sec

VIII. Repeat Liftoff procedure (IV).

IX. Repeat Photoresist procedure (II) with mask 3
   A. Align with alignment masks and contact pads
   B. Make sure mask away from array
   C. Hard bake resist for 60 min in 120C oven

X. Etch nitride
   A. BHF 10:1 at greater than 500A/min
   B. DI Rinse
   C. Soak in acetone
   D. Cleaning procedure I.

References

[1] M. Exter and D. Grischkowsky, "Carrier dynamics of electrons and holes in moderately doped silicon", *Phys. Rev. B*, Vol. 41, No. 17, pp. 12140-9, 1990.

[2] N. Katzenellenbogen, D. Grischkowsky, "Electrical characterization to 4 THz of N- and P-type GaAs using THz time-domain spectroscopy", *Appl. Phys. Lett.*, Vol. 61, No. 7, pp. 840-2, 1992.

[3] M. Exter, C. Fattinger, D. Grischkowsky, "Terahertz time-domain spectroscopy of water vapor", *Opt. Lett.*, Vol. 14, No. 20, pp. 1128-30, 1989

[4] W.J. Walecki, D. Some, V.G. Koslov, A.V. Nurmikko, "Terahertz electromagnetic transients as probes of a two-dimensional electron gas", *Appl. Phys. Lett.*, Vol. 63, No. 113, pp. 1809-11, 1993

[5] J. Son, T.B. Norris, J.F. Whitaker, "Terahertz electromagnetic pulses as probes of transient velocity overshoot in GaAs and Si", *J. Opt. Soc. Am. B*, Vol. 11, No. 12, pp. 2519-27, 1994.

[6] P.R. Smith, D.H. Auston, M.C. Nuss, "Subpicosecond Photoconducting Dipole Antennas", *IEEE J.Q.E.*, Vol. 24, No. 2, pp. 255-260, 1988.

[7] P.K. Benicewicz and A.J. Taylor, "Scaling of Terahertz radiation from large-aperture biased InP photoconductors", *Opt. Lett.*, Vol. 18, No. 16, pp. 1332-4, 1993.

[8] D.You, R.R. Jones, P.H. Bucksbaum, and D.R. Dykaar, "Generation of high-power sub-single-cycle 500fs electromagnetic pulses", *Opt. Lett.*, Vol. 18, No. 4, pp. 290-2, 1993.

[9] E. Budiarto, J. Margolies, S. Jeong, J. Son, J. Bokor, "High Intensity THz Pulses at 1 kHz Repetition Rate", submitted for publication.

[10] A.R. von Hippel, *Molecular Science and Molecular Engineering*, The Technology Press of MIT and John Wiley and Sons, New York, pp. 39-47, 1959.

[11] S.E. Ralph and D. Grischkowsky, "Trap-enhanced electric fields in semi-insulators: The role of electrical and optical carrier injection", *Appl. Phys. Lett.*, Vol. 59, No. 16, pp. 1972-74, 1991.

[12] E. Budiarto, J. Margolies, S. Jeong, J. Son, J. Bokor, "High Intensity THz Pulses at 1 kHz Repetition Rate", submitted for publication.

[13] A. Yariv and P. Yeh, *Optical Waves in Crystals*, New York, Wiley, 1984, ch. 7.

[14] B.H. Kolner, D.M. Bloom, "Electrooptic Sampling in GaAs Integrated Circuits", *IEEE J.Q.E.*, Vol. QE-22, No. 1, pp. 79-93, 1986.

[15] Joseph W. Goodman, *Introduction to Fourier Optics*, 2nd ed., McGraw-Hill, 1995, pg. 47.

[16] J.T. Darrow, X.-C. Zhang, D.H. Auston, "Saturation Properties of Large-Aperture Photoconducting Antennas", IEEE J.Q.E., Vol. 28, No. 6, pp1607-15, 1992.

[17] A. J. Taylor, P.K. Benicewicz, S.M. Young, "Modeling of femtosecond electromagnetic pulses from large-aperture photoconductors", Opt. Lett., Vol. 18, No. 16, pp1340-2, 1993

[18] Amnon Yariv, *Quantum Electronics*, Third Edition, John Wiley and Sons, New York, 1989, p119.

[19] Amnon Yariv, *Quantum Electronics*, Third Edition, John Wiley and Sons, New York, 1989, p123.

[20] D.You, R.R.Jones, P.H.Bucksbaum, and D.R.Dykaar, "Generation of high-power sub-single-cycle 500fs electromagnetic pulses", Opt.Lett., Vol. 18, No. 4, pp. 290-2, 1993.

[21] E. Budiarto, J. Margolies, S. Jeong, J. Son, J. Bokor, "High Intensity THz Pulses at 1 kHz Repetition Rate", submitted for publication.

[22] N.M. Froberg, B.B. Hu, X.-C. Zhang, D.H. Auston, "Terahertz Radiation from a Photoconducting Antenna Array", IEEE J.Q.E., Vol. 28, No. 10, pp. 2291-2301, 1992.

[23] J.W. Goodman, Statistical Optics, John Wiley and Sons, New York, 1985, p206.